applied sciences

MDPI

Article

Effect of Liquid Properties on the Characteristics of Collisions between Droplets and Solid Particles

Anastasia Islamova, Pavel Tkachenko, Nikita Shlegel and Geniy Kuznetsov *

Heat Mass Transfer Laboratory, National Research Tomsk Polytechnic University, Tomsk 634050, Russia
* Correspondence: kuznetsovgv@tpu.ru; Tel.: +7-(3822)-701-777 (ext. 1615)

Abstract: The characteristics of the collisions of droplets with solid particles (52,100 steel) were experimentally studied when varying the key liquid properties: viscosity (1–6.3 mPa·s), surface tension (72.69–36.1 mN/m) and interfacial (liquid-liquid) tension (3.41–42.57 mN/m). Distilled water, aqueous solutions of glycerol, surfactants and diesel emulsions were used. The experimental conditions corresponded to the following ranges: Weber number 5–450, Ohnesorge number 0.001–0.03, Reynolds number 0.1–1000, capillary number 0.01–0.3. Droplet-particle collision regimes (agglomeration, stretching separation) were identified and the characteristics of secondary liquid fragments (size, number) were determined. Droplet-particle interaction regime maps in the We(Oh) and Re(Ca) systems were constructed. Equations describing the transition boundaries between the droplet-particle interaction regimes were obtained. The equations take the form: $We = a \cdot Oh + c$. For the conditions of the droplet-particle interaction, the relationship $We = 2214 \cdot Oh + 49.214$ was obtained. For the interaction with a substrate: $We = 1.0145 \cdot Oh + 0.0049$. The experimental results were compared with the characteristics of collisions of liquid droplets with each other. Differences in the characteristics of secondary atomization of droplets as a result of collisions were identified. Guidelines were provided for applying the research findings to the development of liquid droplet secondary atomization technologies in gas-vapor-droplet applications.

Keywords: liquid droplets; solid particles; collisions; interaction regimes; liquid properties; child droplets

Citation: Islamova, A.; Tkachenko, P.; Shlegel, N.; Kuznetsov, G. Effect of Liquid Properties on the Characteristics of Collisions between Droplets and Solid Particles. *Appl. Sci.* **2022**, *12*, 10747. https://doi.org/10.3390/app122110747

Academic Editor: Gaind P. Pandey

Received: 5 October 2022
Accepted: 21 October 2022
Published: 24 October 2022

1. Introduction

Investigating the patterns of the interaction of liquid droplets with solid surfaces as illustrated by substrates and particles is of special importance. Several numerical and experimental studies on the interaction of droplets of water [1], solutions [1,2], emulsions [3] and slurries [4–6] with substrates and particles from different materials, such as steel [3,7] and glass [8,9], have been published. The considerable interest in these processes is conditioned by a wide range of their applications in, e.g., chemical and heat exchange technologies [10–12], pharmaceutical industry [13,14], food industry [15,16], firefighting [17,18], thermal treatment of water [19,20], spraying technologies [21,22], etc. Experimental research into the collisions of liquid droplets with solid particles is carried out using several approaches [23]. The most popular approaches involve the generation of a droplet in free fall on a fixed particle [24–26], simultaneous movement of droplets and particles [27,28] and identification of the interaction of droplets with particles in two- and multiphase flows. To date, the effect of a group of factors and parameters on the regimes and outcomes of the interaction of liquid droplets with solid particles has been experimentally studied [23,28,29] using the above approaches. These parameters include the sizes, velocities, impact angles and surface properties (wettability, roughness) of particles and substrates [30]. The following regimes of droplet–particle interaction are usually distinguished [23]: agglomeration, stretching separation and stretching separation with the formation of a different number of satellite droplets of varying sizes. Theoretical studies made it possible to establish the

effect of such major parameters as surface wettability [31,32], Weber number [31,33–35], Reynolds number [36], droplet-to-particle size ratio [31], surface curvature [35,37], droplet diameter and liquid viscosity [8] on the outcomes of the droplet–particle interaction. The present-day ideas of the patterns of interaction of liquid droplets with solid particles are shaped by the experimental and theoretical studies such as [35,38,39]. They present typical collision regime maps for liquid droplets and solid particles. The critical Weber, Reynolds, Ohnesorge and capillary numbers were shown, at which a collision regime changes.

Among the key parameters affecting the droplet-particle interaction, the properties of liquid (its viscosity, density, surface and interfacial tension) are especially interesting to explore in the context of their effect on the interaction. This is because the multicomponent liquids used in technical applications vary greatly in their viscosity, surface and interfacial tension. Thus, e.g., research findings [8,40,41] substantiate the crucial role of liquid properties in the characteristics of the interaction of droplets with solid surfaces. Thus, for instance, a lower viscosity of liquid in the collision of a free-falling droplet with a substrate leads to a significant reduction in the size of child droplets [42–44]. Lower surface tension increases the time taken to break up the liquid bridge between particles, which, in turn, has a considerable influence on the impact dynamics and characteristics of droplet spreading over a solid surface [8]. Such effects help promote cost reduction in liquid spraying due to a decrease in the critical Weber number and consequently relative droplet velocities. The joint contribution of different liquid properties is generally described using dimensionless similarity criteria (the Weber, Ohnesorge, Reynolds and capillary numbers). The critical values of these criteria were determined [45] for the regime transition boundaries of droplet-droplet interaction. To supplement the study [45], it is instructive to evaluate the effect of liquid properties on the characteristics of collisions between droplets and solid particles of comparable sizes. It is important to compare the observed effects with equivalent ones when droplets collide with substrates. The findings cited above suggest that, until recently, the combined effect of three essential liquid properties on the characteristics of droplet-particle collisions has not been experimentally studied. This is what became the motivation for this research.

The aim of this research is to build droplet-particle collision regime maps when varying the liquid properties and to compare the obtained findings with the characteristics of interaction of droplets with each other. Following the analysis of the findings, it is important to determine the conditions of rapid disruption of liquid droplets colliding with each other and with solid particles to provide guidelines for the development of technologies of secondary atomization of droplets in different gas-vapor-droplet systems.

2. Materials and Methods

2.1. Materials

In the experiments, a group of liquid compositions was used to understand the impact of liquid properties on the characteristics of droplet-particle collisions. Their properties are listed in Table 1. The viscosity of liquids was determined by means of a Brookfield DV3T LV viscometer [46] at room temperature (20–23 °C).

Table 1. Properties of liquids under study.

Name of Composition	Density ρ, kg/m^3	Surface Tension σ, mN/m	Dynamic Viscosity μ, mPa·s	Interfacial Tension σ_0, N/m
Water	998	72.69	1	–
Compositions to vary μ				
Glycerol solution (10 vol%)	1022	71.3	1.371	–
Glycerol solution (25 vol%)	1060	69.3	2.239	–
Glycerol solution (50 vol%)	1126	66.1	6.301	–

Table 1. *Cont.*

Name of Composition	Density ρ, kg/m^3	Surface Tension σ, mN/m	Dynamic Viscosity μ, mPa·s	Interfacial Tension σ_0, N/m
Compositions to vary σ				
95.5 vol% distilled water and 0.5 vol% Tween-80	998	47.4	1	–
95.5 vol% distilled water and 0.5 vol% Tween-20	998	40.1	1	–
95.5 vol% distilled water and 0.5 vol% neonol	998	36.1	1	–
Compositions to vary σ_0				
10 vol% distilled water, 90 vol% diesel	828	27.5	2.59	42.57
10 vol% distilled water, 90 vol% diesel, 0.08 g/L emulsifier D_cD	828	27.5	2.52	22.49
10 vol% distilled water, 90 vol% diesel, 1.6 g/L emulsifier D_cD	828	27.5	2.43	3.41

Viscosity was measured using a spindle complete with a heat-insulated cylindrical jacket (150 mm high, with an aperture 20 mm in diameter to fit a 50-mL test tube) and a SC4-34 spindle (measurement range 24–600 × 10^3 mPa·s) operating with a Small Sample Adapter (SSA) (heat-insulated with a cylindrical jacket with a built-in chamber for samples with a volume of less than 16 mL). The viscometer with dedicated software measured the shear rate of liquid that was used to calculate its dynamic viscosity. The accuracy of the shear rate measurement was ±1% in compliance with ASTM D445 [47]. To determine the influence of liquid viscosity on the characteristics of atomization of droplets due to their collisions with a solid particle, solutions with varying concentrations of glycerol (10 vol%; 25 vol%; 50 vol%) and distilled water were used. Such solutions made it possible to vary the liquid viscosity (1–6.301 mPa·s).

To explore the impact of liquid surface tension on the regimes and outcomes of the interaction of a droplet with a solid particle, aqueous solutions of surfactants were prepared: 99.5 vol% distilled water and 0.5 vol% Tween-20; 99.5 vol% distilled water and 0.5 vol% Tween-80; 99.5 vol% distilled water and 0.5 vol% neonol. Such solutions made it possible to vary the surface tension of liquid in the range of 36.1–72.69 mN/m. Du Noüy ring method (K6 tensiometer, KRUSS) [48] was used to measure the surface tension of the investigated liquids at 20–23 °C. It ranged from 1.0 to 90.0 mN/m.

To determine the liquid interfacial tension, an ST-2 stalagmometer was used. Its operating principle is based on determining the volume of water droplets forced onto the diesel-with-emulsifier/water interface [49]. D_cD emulsifier was selected to vary the interfacial tension [50]. Summer diesel fuel, distilled tall oil (DTO), triethanolamine (TEA) and diethylamine (DEA) were mixed to produce the emulsifier. The diesel emulsion was prepared in a Sapfir 2.8 ultrasonic bath at a frequency of 35 kHz. At the first stage, D_cD emulsifier was added to diesel fuel at a concentration of 0.08 g/L and 1.60 g/L. The choice of these concentrations was justified in [45]. After that, the components were stirred for 2 min and 10 vol% water was added. The emulsion was stirred for 300 s. The emulsions involved in the research and their preparation procedure are identical to those used in [45].

Spherical metal balls 2–4 mm in diameter were used as solid particles. This size of spherical particle was chosen by varying the surface curvature and determining the size of

particles at which the collision of a droplet with a particle was close to that of a droplet with a flat substrate. Metal substrates in the form of a 10-mm-thick cylindrical disc 80 mm in diameter were also used. The material of particles and substrates was 52,100 bearing steel.

2.2. Experimental Procedures

The experiments were conducted using the setup presented in Figure 1. To vary the droplet size (R_d) from 0.2 to 1.0 mm, detachable nozzles were employed: G17, G21, G25, G30. Droplets of the compositions under study were fed with a SinoMDT SN-50F6 syringe pump (infusion accuracy within 2%, 0.1 mL/h step of infusion rate adjustment, max. flow rate 1500 mL/h). A 50-mL syringe was fit in the pump. Such a pump provided a constant flow rate of liquid of approx. 100 mL/h. A spherical particle was held by a nozzle connected to the vacuum pump. A positioning mechanism controlled the particle height and centricity relative to the droplet. An allowable deviation of centricity in the experiments did not exceed 5% from the initial droplet radius. To adjust the collision centricity, the second high-speed video camera was used. Before each experiment, the particle and substrate surfaces were thoroughly cleaned with isopropyl alcohol to remove traces of liquid from the previous experiment and wiped with a lint-free cloth. In the study of droplet-substrate collisions, the substrate was placed on a lifting table.

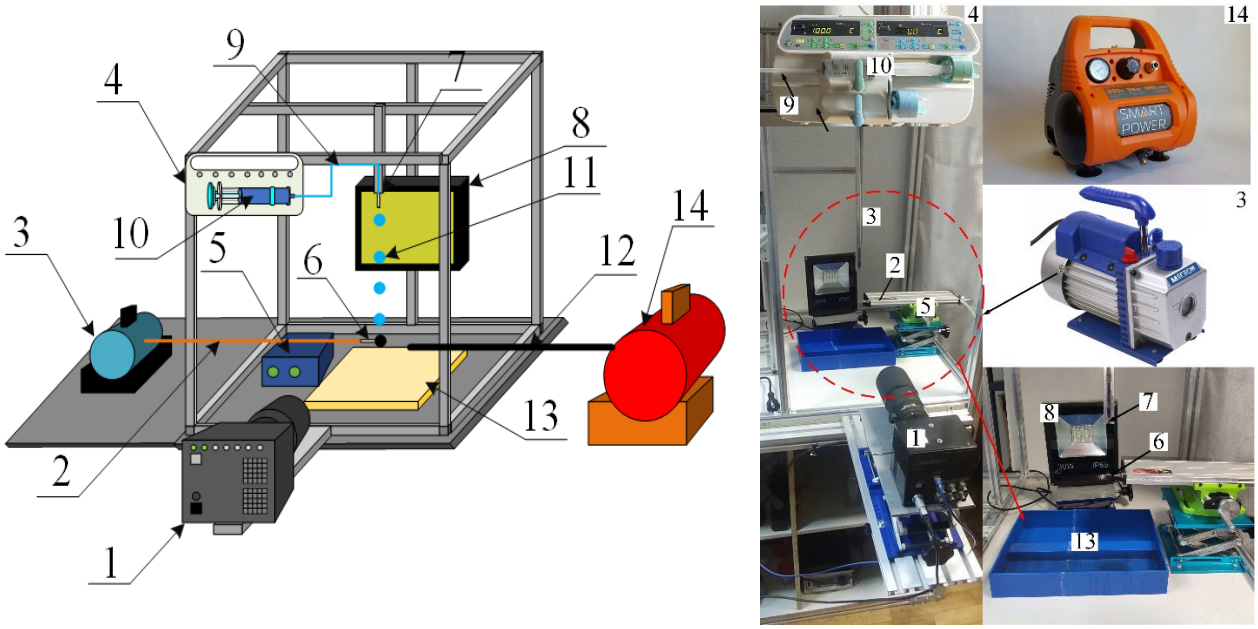

(**a**) (**b**)

Figure 1. Experimental setup scheme (**a**) and photo (**b**): 1—high-speed video camera; 2—copper capillary of vacuum pump; 3—vacuum pump; 4—syringe pump; 5—positioning mechanism; 6—particle holder (a needle with a flat tip); 7—detachable nozzle; 8—spotlight; 9—liquid supply capillary; 10—syringe; 11—liquid droplet; 12—air supply capillary; 13—container to collect liquid; 14—air compressor.

A Fastcam Mini UX100 high-speed video camera with a Sigma 105 mm f/2.8 EX DG OS HSM Macro Nikon F lens was used to record the droplet-particle collisions. The video camera settings during the experiments were as follows: frame rate—5000 fps, resolution—1280 × 1024 pixels, inter-frame delay of 1/25,000. The key parameters of droplet-particle interaction were recorded (Figure 2): droplet radius (R_d); particle radius (R_p); droplet velocity (U_d); distance between the centers of mass of the particle and droplet (b). The systematic measurement error of droplet sizes, velocities and impact angles was 2.1%, 3.4% and 1.8%, respectively. Following the analysis of the images, the Weber number ($We = 2 \cdot \rho \cdot R_d \cdot {U_d}^2/\sigma$), Ohnesorge number ($Oh = \mu/(2 \cdot R_d \cdot \rho \cdot \sigma)^{0.5}$), Reynolds number ($Re = \rho \cdot 2R_d \cdot U_d/\mu$) and capillary number ($Ca = \mu \cdot U_d/\sigma$) were calculated [51]. The

Ohnesorge number reflects the ratio of viscous forces to the combined effect of inertial and surface tension forces. The Weber number is related to the ratio of inertial forces to the surface tension forces. Constructing droplet-particle collision regime maps in the We(Oh) system takes the effect of density, viscosity and surface tension of liquid into account [23]. The linear impact parameter was calculated allowing for the distance between the centers of mass of the particle and droplet: $B = b/(R_d + R_p)$. When establishing the regime boundaries, experimental points were plotted on the map. After that, the terminal or boundary points, characterizing each regime of the droplet interaction, were determined. Then a boundary connecting these points was plotted. If 95% of the points were within the boundary of a certain regime area, an approximation boundary line was drawn. The Weber and Ohnesorge numbers, as well as the linear impact parameter, were calculated. This was followed by producing regime maps in the B(We) coordinate system. The regime maps were plotted using the dimensionless impact parameter, since it also indirectly allows for the impact angle.

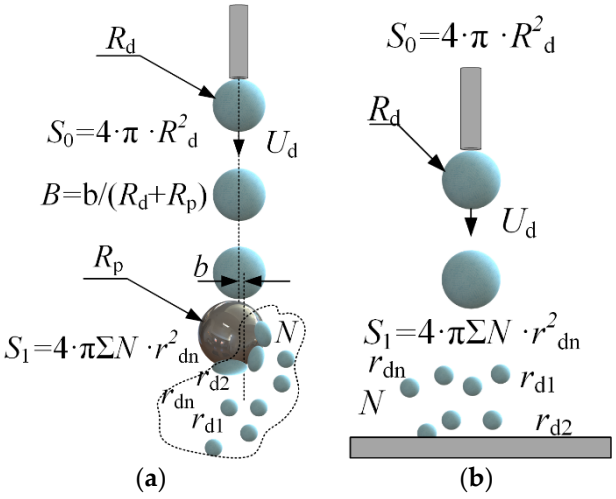

Figure 2. Scheme for calculating the characteristics of droplet-particle (**a**) and droplet-substrate (**b**) collisions.

Droplet fragmentation efficiency was calculated from the ratio of free surface areas after and before the interaction with a particle (S_1/S_0, where $S_1 = 4 \cdot \pi \cdot \Sigma {r_{dn}}^2$—free surface area after the droplet fragmentation, m^2, $S_0 = 4 \cdot \pi \cdot {R_d}^2$—droplet area before fragmentation, m^2) [38]. To that end, the radii (r_{dn}) and number (N) of all the child droplets were measured. The particle-to-droplet size ratio was calculated ($\Delta = R_p/R_d$), as this ratio significantly affects the collision dynamics [23,52].

3. Results and Discussion

3.1. Droplet-Particle Collision Regimes

The analysis of the experimental findings revealed two regimes of the interaction of droplets with solid particles (Figure 3): agglomeration (A) and stretching separation (SS). Sometimes, stretching separation with the formation of several child droplets [23] is additionally identified. In the current study, the transition boundaries between the regimes with a formation of several child droplets were determined. In agglomeration, the droplet-particle collision does not result in child droplet formation. The droplet spreads over the particle surface. At a higher velocity of the initial droplet, it is disrupted and child droplets are produced. In this study, this collision regime was recognized as stretching separation, as in [23]. To explore the way liquid properties affect agglomeration, the time of the droplet spreading over the particle was examined. This was the interval from the time of the droplet-particle contact until the thickness of liquid on the particle surface in the contact point stopped changing.

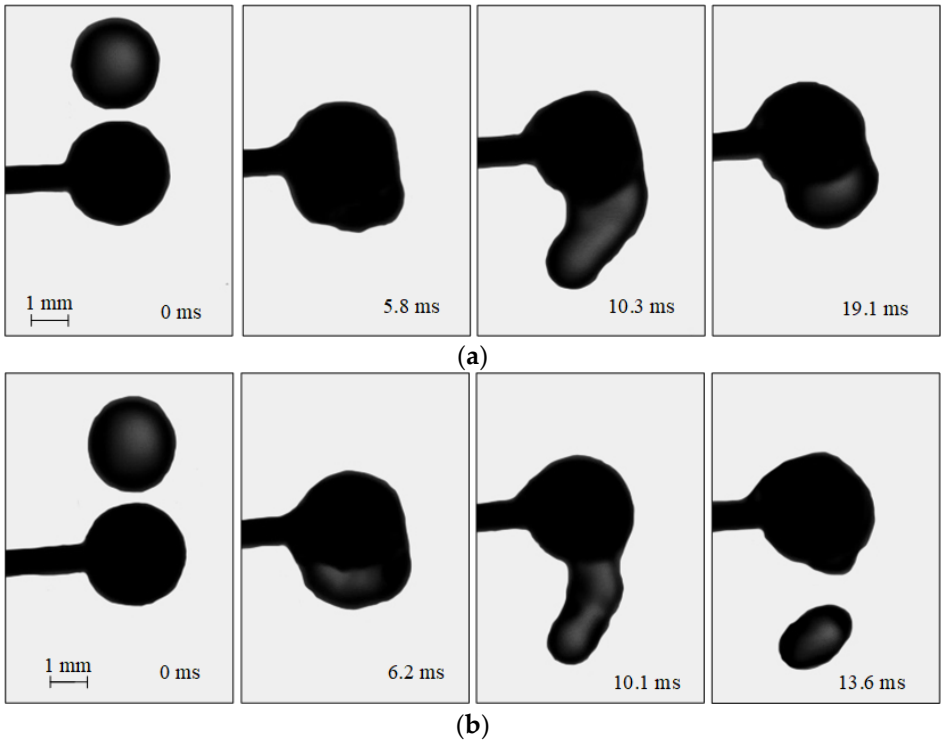

Figure 3. Images illustrating the collisions of water droplets with a particle: (**a**)—agglomeration (R_d = 2.15 mm; R_p = 3 mm, U_d = 2.67 m/s); (**b**)—stretching separation (R_d = 2.2 mm; R_p = 3 mm, U_d = 3.2 m/s).

The duration of agglomeration indicates the efficiency of the solid particle capturing in dust removal (e.g., in venturi scrubbers). The shorter the agglomeration, the more effective the solid particle capturing [53,54]. The duration of the droplet spreading over a solid particle surface also determines the efficiency of the slurry fuel droplet generation in combustion chambers when coal particles, water, oil, biomass, peat, slime, heavy coal-tar products, resins and other components are injected separately [55]. For example, for the 50 vol% and 10 vol% glycerol solutions, there were 8 and 14 child droplets, respectively. The results are consistent with the findings [45].

3.2. Effect of Liquid Viscosity

Figure 4 shows the interaction of particles with droplets at varying dynamic viscosities of liquid. Video S1 contains the corresponding video-grams. It is clear in Figure 4 that, at identical sizes and velocities of droplets before the collision, a lower number of secondary fragments with larger sizes were generated with a higher dynamic viscosity of liquid. For example, for the 50 vol% and 10 vol% glycerol solutions, there were 8 and 14 child droplets, respectively. These results are consistent with the findings [45]. An increase in viscosity leads to greater viscous friction forces in the near-wall boundary the liquid layer. These prevent its spreading over the particle surface. Hence, the liquid-particle contact area is smaller. As a result, a liquid layer with a smaller volume is entrained from the particle surface. The viscous forces prevent its significant deformation during floating. Thus, fewer child droplets result from its breakup. With highly viscous liquids, the newly formed child droplets quickly assumed a spherical shape. That was caused by high internal friction forces that changed the standard deformation cycles of droplets during free fall (prolate ellipsoid—sphere—oblate ellipsoid—sphere, etc.) and by surface tension forces of liquid, preventing its deformation. The observed effects also led to a smaller area of separation of child droplets after a highly viscous liquid contacted a particle compared to the equivalent characteristic in the experiments with water droplets. More viscous liquids spend greater

energy on overcoming viscous friction. Thus, the child droplets had lower velocity when breaking off from the spherical particle.

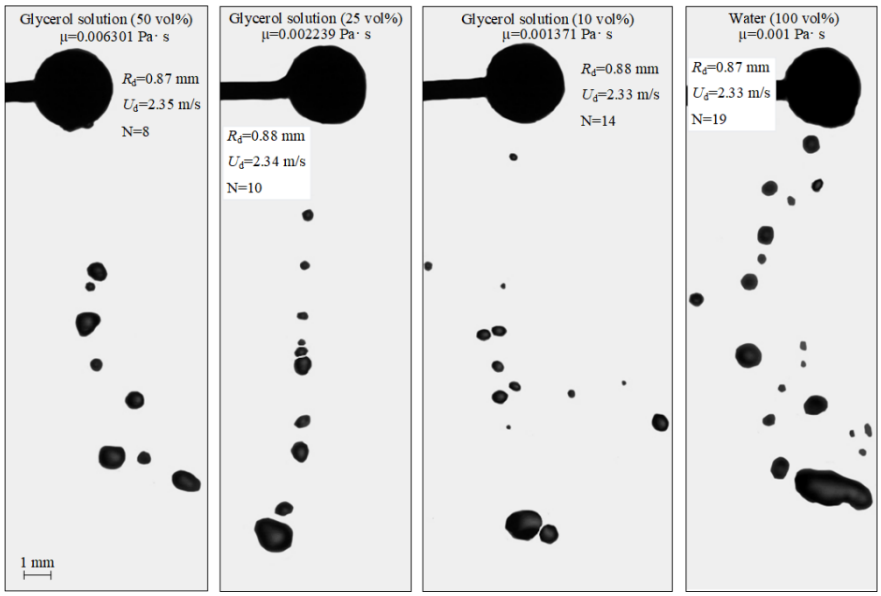

Figure 4. Images illustrating the collisions of water droplets with a particle in the stretching separation regime at varying liquid viscosities.

Figure 5a presents a collision regime map for water and glycerol solution droplets interacting with a metal particle approx. 3 mm in diameter. A dimensionless linear impact parameter (B) was used to construct the regime maps. This allowed for the radii of droplets and particles, the centricity of droplet-particle interaction and the Weber number, related to inertia and surface tension, droplet velocity and sizes. An increase in the liquid viscosity was found to significantly shift the boundary between agglomeration and stretching separation towards higher Weber numbers (Figure 5a).

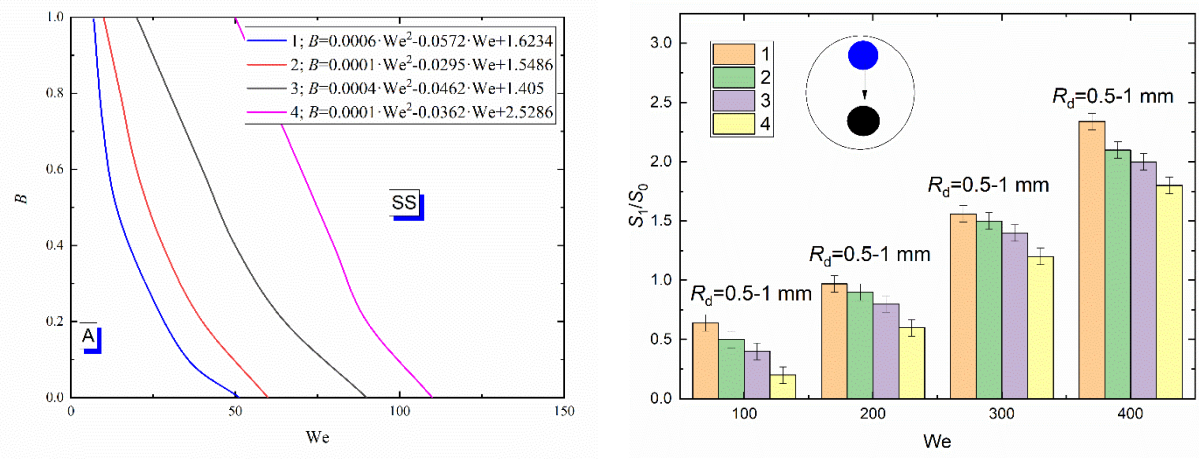

(**a**) (**b**)

Figure 5. Collision regime maps for liquid droplets interacting with solid particles (**a**) and ratios of free surface areas after (S_1) and before (S_0) the head-on collision with B = 0 (**b**) at varying viscosities of liquid and constant size of droplets: 1—distilled water; 2—10 vol% glycerol solution; 3—25 vol % glycerol solution; 4—50 vol % glycerol solution.

Thus, at identical R_d, B, α and ambient gas temperature, the boundary of stretching separation for water droplets corresponds to We = 20 and for the 50 vol% glycerol solution

to 75. Consistent occurrence of stretching separation for the composition with higher viscosity is provided by increasing the droplet velocity. Changes in the viscous forces due to varying concentrations of glycerol in the aqueous solution cannot significantly change the balance of forces. Forces caused by surface tension remain dominant. An increase in the liquid viscosity generally increases the critical Weber number by 20–30%. For boundaries of transition plotted for agglomeration and stretching separation, approximations were obtained like $B = a \cdot We^2 + b \cdot We + c$. They are presented in Figure 5. To plot the transition boundaries, the terminal or boundary points were determined that characterize the transition between droplet interaction regimes. If 95% of points were within the area of a chosen regime, an approximation curve for the boundary between regimes was plotted. Child droplet trajectories are affected by a set of factors. The key factors are the relative velocity of droplets and particles (that allows for the impact angle), dimensionless linear impact parameter B and the droplet-particle size ratio. It was established that the direction of the child droplet movement after the collision of a droplet with a spherical particle is also affected by the droplet-particle size ratio.

When studying the effect of liquid viscosity on agglomeration, it is important to estimate the duration and, thus, rates of droplet spreading over the particle surface. Such parameters help estimate the duration of agglomeration, i.e., the time that it takes for the liquid droplet to completely envelop the solid particle. The research revealed that an increase in liquid viscosity leads to 25–45% longer interaction times. For instance, when a distilled water droplet collided with a steel particle, the interaction time was 19 ms. For the 50 vol% glycerol solution, this was 27 ms, which leads to the conclusion that, in the particle–droplet collision, a decrease in the liquid viscosity results in a shorter duration of interaction and higher rates of liquid spreading over the particle surface. This also implies that the contact angle increases without a change in surface properties. An increase in the contact angle is related to a higher surface tension of liquid.

In the experiments with higher liquid viscosity, there were larger child droplets, which led to a reduction in their number compared to the experiments with distilled water droplets. The satellite droplets resulting from the fragmentation of liquid droplets with higher viscosity assumed a spherical shape faster than those resulting from the fragmentation of water. This effect is related to the dominance of viscous forces over rotational forces, which leads to a lower duration and narrower range of child droplet shape change in deformation cycles [56]. Since highly viscous liquid droplets tend to assume a spherical shape, they are less susceptible to deformation when moving in gas environment. Thus, they hardly break up, which results in the formation of larger child droplets. This phenomenon decreases the ratio of the free surface area of the liquid after and before the fragmentation caused by the droplet-particle contact. Figure 5b clearly shows that, with an increase in the liquid viscosity from 1.0 to 1.4 mPa·s, S_1/S_0 decreases by almost 25–35% within the whole Weber number range under study. This trend persists with a further increase in the liquid viscosity from 1.4 to 6.3 mPa·s. The ratios of areas after and before the collision are steadily decreasing.

3.3. Effect of Liquid Surface Tension

The images illustrating the effect of surface tension on the regimes and outcomes of the collisions of droplets with a solid particle are presented in Figure 6 and Video S2.

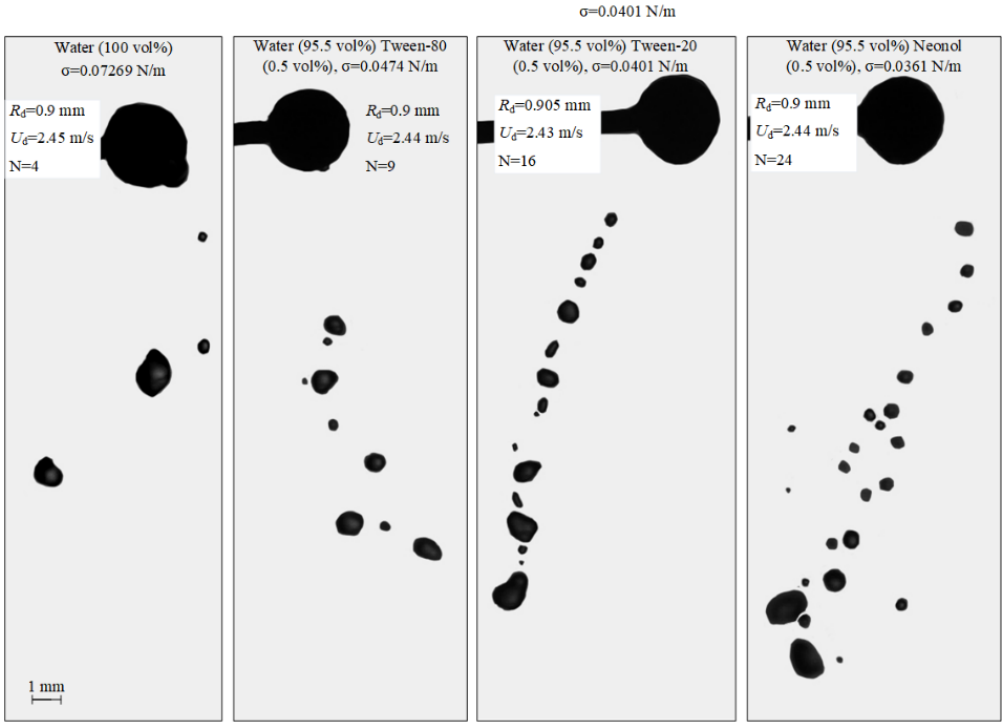

Figure 6. Images illustrating the collisions of liquid droplets with a particle in the stretching separation regime at varying liquid surface tensions.

Adding a surfactant to water reduces the surface tension almost twofold, which, in turn, increases the number of child droplets. In particular, adding a surfactant (0.5 vol% Tween-80) to distilled water reduces the surface tension from 72.69 to 47.4 mN/m. This increases the number of satellite droplets almost twofold. A reduction in the liquid surface tension causes inertia to dominate the surface tension forces of the liquid. Moreover, a decrease in the surface tension at the liquid–gas interface suggests a directly proportional reduction in the energy required to break up the specific surface. This effect leads to a more substantial transformation of the surfactant solution droplets compared to water droplets. When a surfactant solution droplet lands on a particle, it spreads over the surface and breaks up into a great number of child droplets. Similar conclusions were made in [8], where a decrease in the surface tension was shown to intensify the droplet spreading over the surface. When droplets broke up from a collision with a particle, there were no fragments of a spherical shape. Practically all the secondary fragments actively transformed during floating, assuming the shape of ellipsoids of revolution with variable amplitudes and temporal deformation cycles.

It is clear in Figure 7a that the shift of the separation regime boundaries towards lower (by 15–25%) critical Weber numbers is caused by lowering the surface tension of the liquid almost twice. The results presented in Figure 7a indicate that a slight decrease in the liquid surface tension (from 0.0474 to 0.0361 N/m) almost does not affect the interaction regime maps (the changes being no more than 3%). At the same time, when the liquid surface tension becomes 35–55% lower, the time of the liquid droplet-particle interaction in the agglomeration regime decreases, i.e., the spreading rate increases. For example, the spreading time of a distilled water droplet over a particle is approx. 19 ms, that of the Tween-20 solution is 11 ms. A key specific aspect was identified. A further decrease in the liquid surface tension (from 0.0474 to 0.0361) has no significant impact on the spreading time of droplets over a particle (the changes do not exceed 5%). This suggests that a lower liquid surface tension significantly affects the duration of the droplet-particle interaction in the agglomeration regime: it reduces the interaction time and increases the spreading rate. The specified aspects are important to predict the conditions of changes (considerable and

inconsiderable) on the droplet-particle collision regime maps when using liquids that have different rheological and surface-active properties.

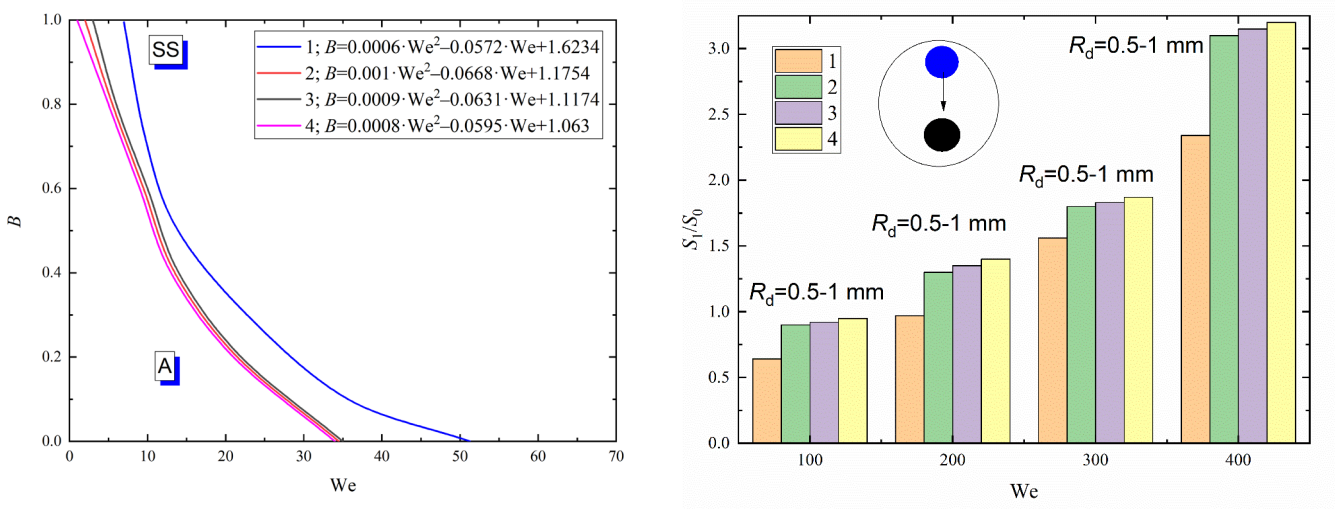

(**a**) (**b**)

Figure 7. Collision regime maps for liquid droplets interacting with solid particles (**a**) and ratios of free surface areas after (S_1) and before (S_0) the head-on collision with $B = 0$ (**b**) at varying liquid surface tensions: 1—distilled water; 2—0.5 vol% Tween-20 and 95.5 vol% water; 3—0.5 vol% Tween-80 and 95.5 vol% water; 4—0.5 vol% neonol and 95.5 vol% water.

Figure 7b shows the ratios of the free surface areas after and before the atomization of liquid droplets as a result of their contact with a particle when varying their surface tension. Lower surface tension of liquid was found to increase the number of resulting fragments. In turn, this led to a higher ratio of S_1 to S_0 within the whole Weber number range. For instance, a reduction in the liquid surface tension from 0.07269 to 0.0361 N/m increases S_1/S_0 by 30–45%. This is accounted for by the conversion of some energy spent on overcoming the surface tension forces to kinetic energy. These effects become weaker at a higher relative velocity of droplets, since the kinetic energy in the contact zone of droplets is already high. The experiments showed a significant surface transformation before the interaction (in the amplitude, rotation time and shear deformation) of solution droplets compared to water droplets. Droplets generally assumed an ellipsoidal shape, which is due to weaker surface tension forces that cannot hold the near-surface layers. A droplet with such a shape collided with a particle and was destroyed. The resulting child droplets also fragmented when continuing their movement in gas environment. There is evidence to suggest that a decrease in the liquid surface tension contributes to lower critical velocities (thus, lower We) sufficient for stretching separation to occur compared to distilled water droplets.

3.4. Effect of Interfacial Tension of Liquid

The impact of the interfacial tension of liquid on the characteristics of droplet-particle collisions can be explored for multicomponent compositions. In the atomization of such liquid droplets, not only the internal forces of inertia, but also the molecular bonds contribute greatly to the occurrence of stretching separation. The higher the interfacial tension, the stronger the molecular bonds [45]. Industrial plants, normally using multicomponent liquids, should provide the conditions (by varying the interfacial tension in the given ranges) when stretching separation dominates. This would increase the area of liquid spraying and reduce the average size of liquid fragments. The images demonstrating the effect of the liquid interfacial tension on the characteristics of droplet-particle collisions are presented in Figure 8 and in Video S3.

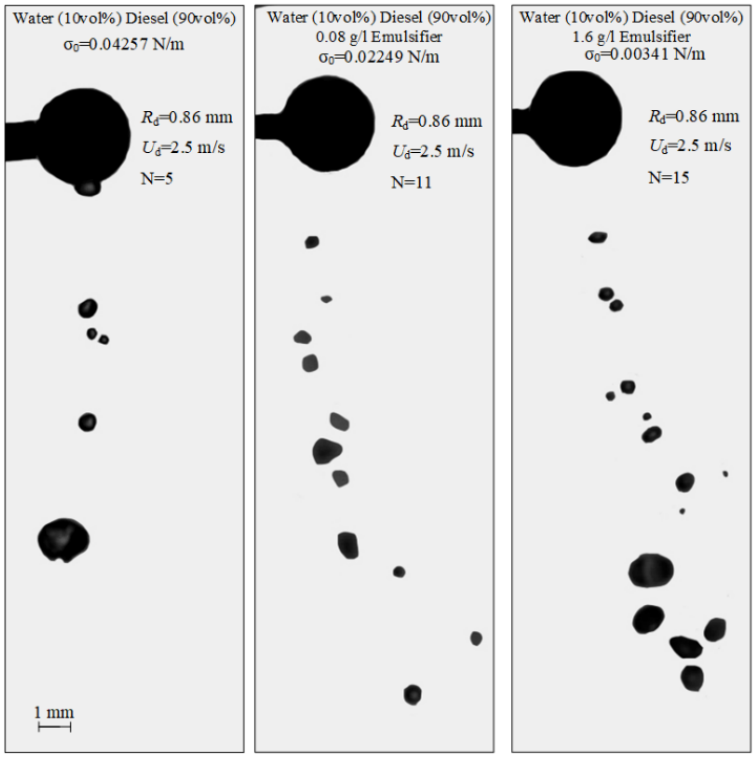

Figure 8. Images illustrating the collisions of water droplets with a particle in stretching separation regime at varying interfacial tensions of liquid.

Shlegel et al. [45] studied the patterns of collisions of liquid droplets with each other at variable rheological properties. It was established [45] that a decrease in the interfacial tension contributes to smaller sizes of internal water droplets in the diesel fuel layers, which makes the emulsion more homogeneous. It is believed that in the collision of diesel emulsion droplets with a solid particle when the liquid contains 0.8–1.6 g/L emulsifier, this effect contributes to a reduction in the child droplet size by up to 30% compared to water. The child droplet number here increases. For example, for diesel emulsion droplets (10 vol% diesel, 90 vol% water) without an emulsifier, there are five child droplets. For emulsion droplets with 1.6 g/L emulsifier, their number reaches 15 at identical initial velocities and sizes of droplets.

The greatest shift in the transition boundaries between stretching separation and agglomeration was recorded (Figure 9a) for droplets of the diesel emulsion with an emulsifier D_cD (1.6 g/L). This is because D_cD increases the stability of the emulsion (i.e., reduces delamination) [45], strengthening the molecular bonds. Lower inertia forces, thus, lower transient Weber numbers are required to break up such emulsion. A high concentration of an emulsifier significantly reduces the surface tension at the liquid–air and liquid–liquid interface. This means that less energy is necessary for the deformation of specific surfaces on both interfaces. Thus, less kinetic energy (Figure 9a) and lower Weber numbers will be required for the liquid droplet dispersion. The comparison of regime maps of diesel fuel emulsions and distilled water reveals a 20–40% decrease in the critical Weber number for the occurrence of stretching separation within the whole range of B. The experiments established that the interfacial tension of liquid has a modest impact on the duration of the droplet spreading over the particle surface, and thus on the spreading rates. For instance, with a decrease in the liquid interfacial tension from 0.04257 to 0.00341 N/m, the droplet spreading time decreases by only 4–7%.

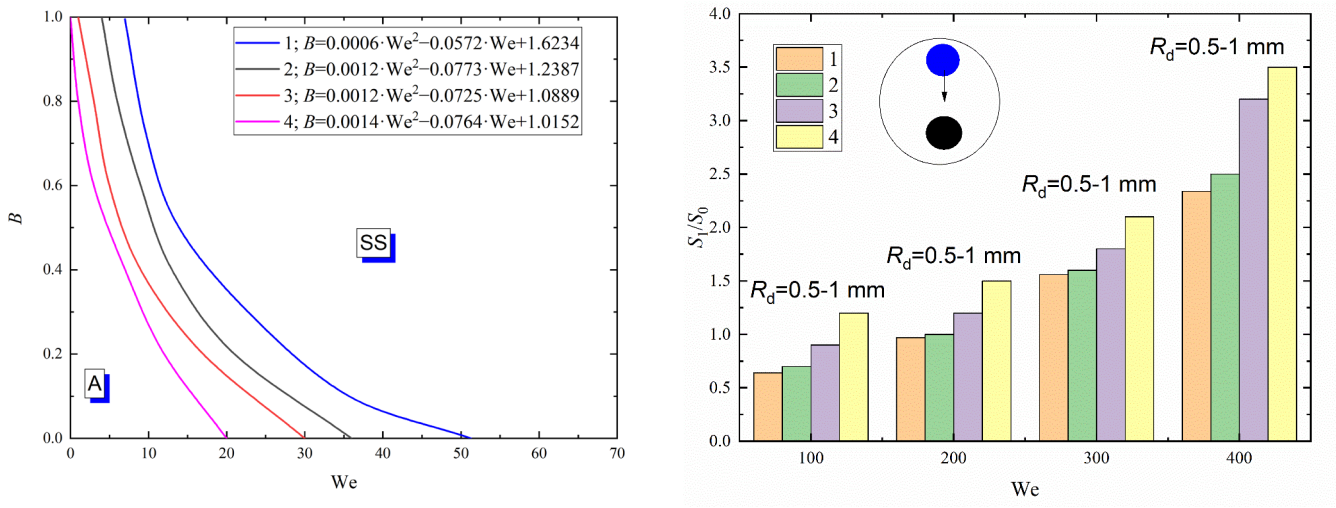

Figure 9. Collision regime maps for liquid droplets interacting with solid particles (**a**) and ratios of free surface areas after (S_1) and before (S_0) the head-on collision with $B = 0$ (**b**) at varying interfacial tensions of liquid: 1—distilled water; 2—90 vol% diesel and 10 vol% water; 3—90 vol% diesel, 10 vol% water and 0.08 g/L emulsifier D_cD; 4—90 vol% diesel, 10 vol% water, and 1.6 g/L emulsifier D_cD.

Figure 9b shows a major impact of the interfacial tension of liquid on the ratio of S_1 to S_0 as a result of its interaction with a solid particle. At minimum interfacial tension, the number of newly formed fragments was found to be maximum. Thus, the S_1/S_0 ratio increased. Such pattern is observed within the whole Weber number range under study. For instance, with a decrease in the interfacial tension from 0.04257 to 0.00341 N/m, the S_1/S_0 ratio increases by almost 30–45%.

3.5. Comparison of Secondary Atomization Methods

To generalize the research findings and compare the methods of secondary atomization (disruption of liquid droplets as a result of their interaction with each other, with particles and substrates), collision regime maps for droplet–particle and droplet–droplet interaction were plotted in the We(Oh) coordinates (Figure 10). The generalization of the findings using the We and Oh numbers simultaneously allows for the surface tension, inertia and viscous forces, as well as the initial droplet size and velocities. The position of the agglomeration and stretching separation boundary was established on the interaction regime maps of liquid droplets colliding with a solid particle (Figure 10a), with each other (Figure 10b) and with a massive substrate (Figure 10c). The comparative analysis of regime maps presented in Figure 10a,b showed that an increase in the Ohnesorge number leads to an increase in the critical Weber number at which the stretching separation occurs when applying both methods of secondary atomization of droplets. For example, the maximum critical Weber number was recorded for the solution with the highest Oh, i.e., the glycerol solution (50 vol% glycerol, 50 vol% water). This suggests that irrespective of the method used to atomize a highly viscous liquid droplet, a similarity criterion like the Ohnesorge number is constant and corresponds to the range of 0.02–0.04. It was established that the Weber numbers necessary for stretching separation during the collision of highly viscous liquids with each other are almost 40% lower than those during the collision between droplets and a particle.

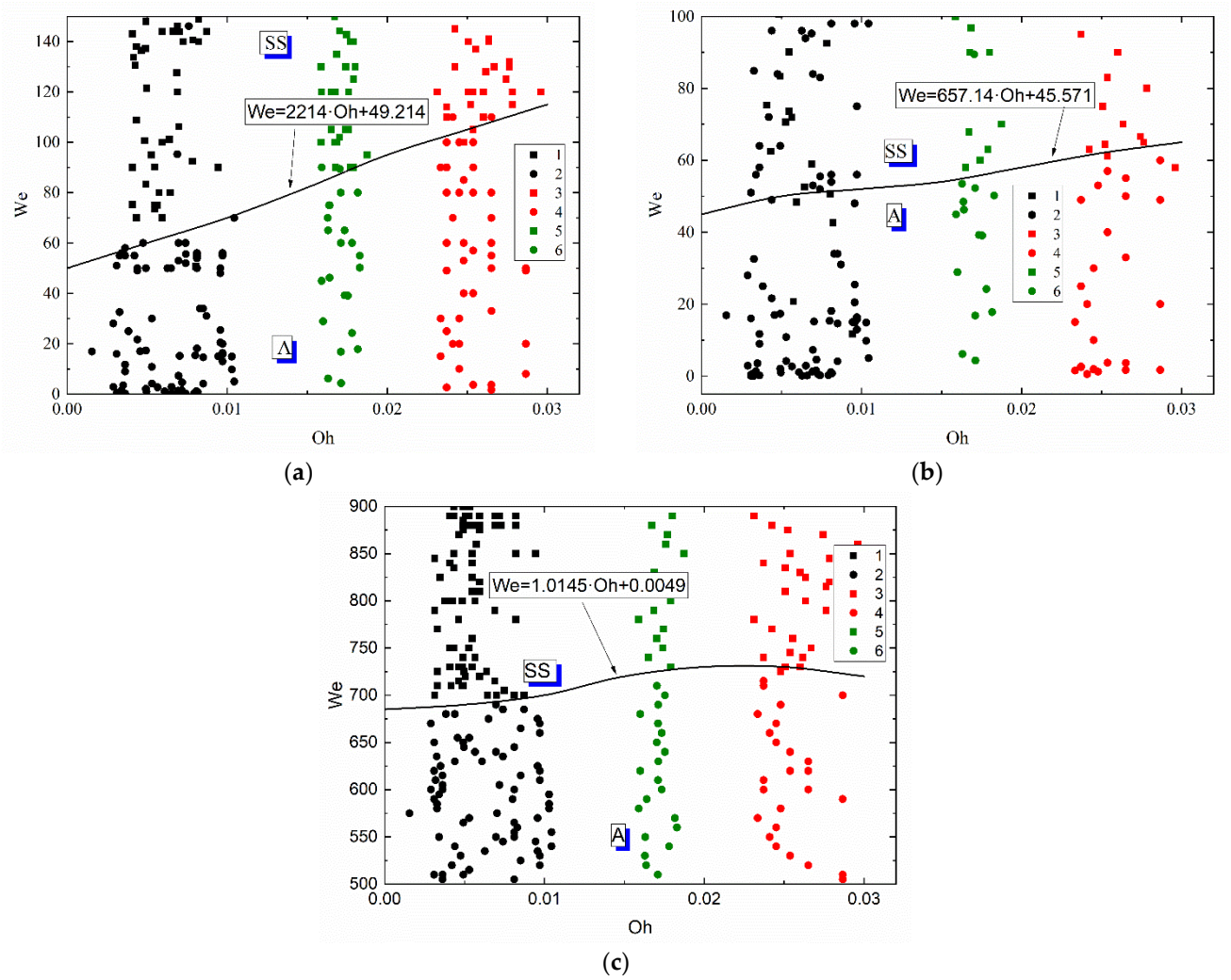

Figure 10. Effect of liquid properties on the transition boundary between agglomeration and stretching separation during the collision of a droplet with a particle (**a**), with another droplet (**b**) [45] and with a solid substrate (**c**): 1, 2—water; 3, 4—50 vol% water and 50 vol% glycerol; 5, 6—10 vol% water and 90 vol% diesel; 1, 3, 5—stretching separation; 2, 4, 6—agglomeration.

The comparison of the schemes of droplet–substrate collisions with those of droplet-droplet and droplet–particle collisions revealed that much higher Weber numbers are required for stretching separation (Figure 10c). This effect stems from the fact that, during a collision of a liquid droplet with a solid substrate, the stretching separation regime occurs consistently at much higher velocities of the initial droplet (almost 3–5 times as high as in its collision with a solid particle). The main difference is in the conditions and area of contact of liquid with a solid surface in the experiments with a substrate and particle. In the experiments with particles, the surface-active forces, the viscous friction and gravity forces cause the liquid to envelop the particle from all sides. The area of contact increases, a layer of liquid is entrained from the particle surface and is broken off to produce a group of child droplets. When a droplet collides with a substrate, the droplet spreads over the surface and the stain of contact increases but later decreases due to the effect of surface forces restoring the droplet shape on the substrate. This is followed by a slow gradual spreading of liquid on the surface. In the case of the atomization of droplets as a result of their interaction with each other and with a massive surface (a solid substrate), the change in the critical Ohnesorge number was similar. Based on the collision regime maps, approximations like We = a · Oh + c were obtained. These equations describe the transition boundaries between agglomeration and stretching separation. It is clear in Figure 10 that

the curve separating agglomeration and stretching separation illustrates a steady growth with an increase in the Oh numbers. Therefore, the form of the boundary (namely, the necessary and sufficient conditions for the transition from one regime to another) on the We(Oh) map can be expected to be the same for any other liquid compositions with varying dynamic viscosities, densities, surface and interfacial tensions.

The experimental research findings presented in this study for the collisions of liquid droplets with solid substrates at varying liquid properties are consistent with the data and conclusions drawn in [57], where coal-water fuels were the investigated liquids. Similarly to [57], a twofold decrease in the surface tension of liquid was found to reduce the critical Weber number between agglomeration and stretching separation almost by 30–40% and increase the number of child droplets 5–7 times. Lowering the interfacial tension makes it possible to decrease the critical Weber number by 35–40% and increase the number of child droplets 5–6 times. An increase in the liquid viscosity from 1 to 6.3 mPa·s in the collision of a droplet with a substrate [57] results in larger child droplets in the same way as it does in the collisions of droplets with each other and with a solid particle. This reduces the number of secondary fragments almost by 10–15%. An increase in the liquid viscosity also shifts the boundary between agglomeration and stretching separation towards 20–30% higher Weber numbers.

Figure 11 attempts to present the regime maps of interaction of droplets with each other (Figure 10b), with a solid particle (Figure 10a) and substrate (Figure 10c) when using such similarity criteria as the Reynolds and capillary numbers. The analysis of the conditions and ranges of the key liquid property variations makes it possible to identify the ranges of consistent occurrence of each of the interaction regimes. For that, the research findings were generalized in the form of Re(Ca) regime maps. Depending on Ca and Re, transitions from agglomeration to stretching separation were recorded. It was established that at high Ca and Re, stretching separation occurs consistently. Collision regime maps in the We(Oh) and Re(Ca) coordinates make it possible to determine the Oh, Ca, Re and We variation ranges (Figures 10 and 11) for agglomeration and stretching separation. These numbers make it possible to factor in the inertia, viscous friction and surface tension forces. Such parameter of liquid as dynamic viscosity was found to have a significant effect on the critical Reynolds number. A rise in the dynamic viscosity reduces the Reynolds number for the transition from agglomeration to stretching separation for all the collisions schemes under study. For instance, an increase in viscosity from 1.0 to 6.3 mPa·s reduces the critical Reynolds number by 10–20%. The analysis of the obtained capillary numbers revealed that a twofold decrease in the liquid surface tension increases Ca by 15–25% in the transition from agglomeration to stretching separation for all the three schemes of droplet collisions.

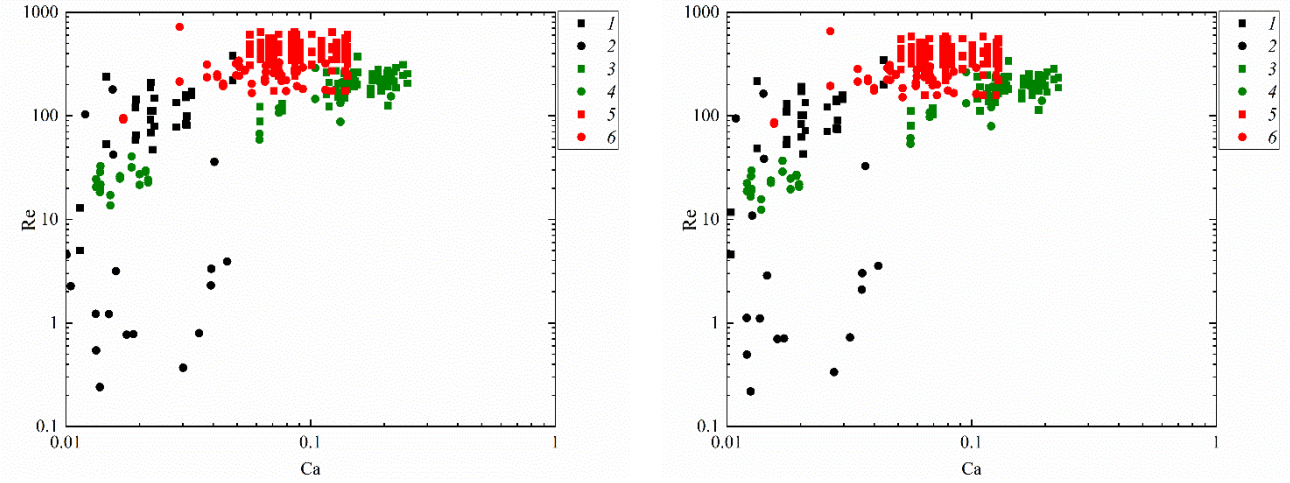

Figure 11. *Cont.*

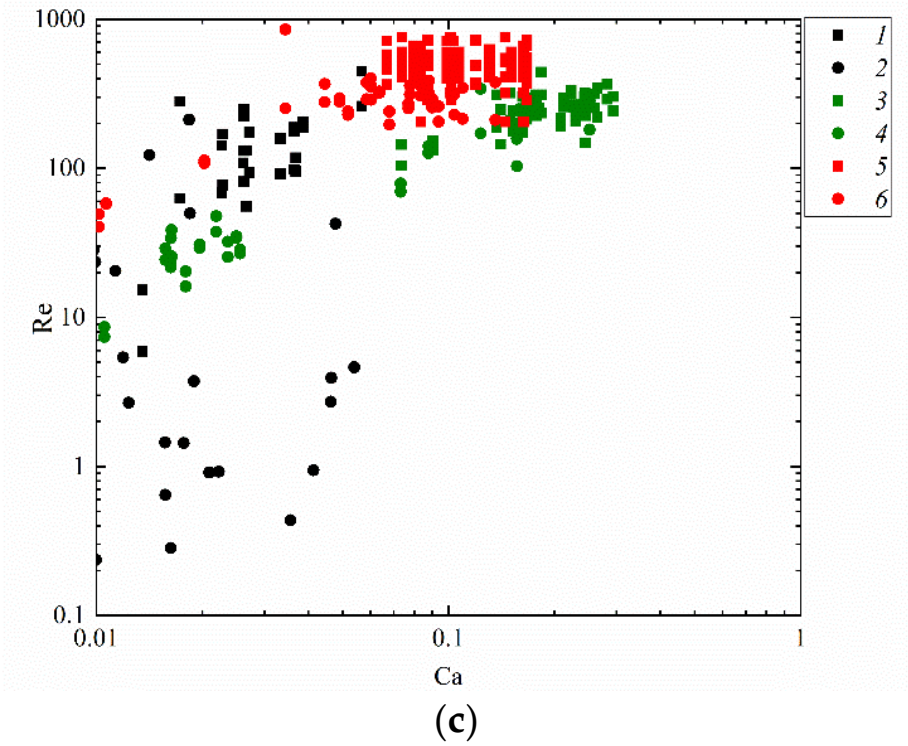

Figure 11. Effect of liquid properties on the transition boundary between agglomeration and stretching separation during the collision of a droplet with a solid particle (**a**), with another droplet (**b**) [45] and with a solid substrate (**c**): 1, 2—water; 3, 4—50 vol% water and 50 vol% glycerol; 5, 6—10 vol% water and 90 vol% diesel; 1, 3, 5—stretching separation; 2, 4, 6—agglomeration.

Studies into the interaction of liquid droplets with a solid particle are associated with certain challenges in conducting experiments. These are generation of micron-sized droplets and particles, providing conditions that are closest to industrial plants (in temperature, pressure, etc.) This makes it necessary to change from experiments over to mathematical modeling of the interaction between liquid droplets and solid particle. Such models should factor in the whole complex of processes identified in the conducted experiments with droplet-particle collisions. A special emphasis is placed here on the calculation of energies in the droplet-particle interaction zone. To calculate the kinetic dissipation energy (E_c) in the droplet-particle collision zone, the following equations [8] are applied:

$$E_p = (\int_{hc}^{h0} F_p \, dh + \int_{h0}^{hrup} F_p \, dh)/E_i; \; F_p = -\int_s pi_z \cdot nds, \quad (1)$$

$$E_{vis} = (\int_{hc}^{h0} F_{vis} \, dh + \int_{h0}^{hrup} F_{vis} \, dh)/E_i; \; F_{vis} = \mu \int_s \nabla u \cdot nds, \quad (2)$$

$$E_{sf} = F_{sf} \cdot (h_{rup} - h_c)/E_i; F_{sf} = 2\sigma R_p \sin(\alpha)\sin(\alpha + \theta), \quad (3)$$

$$E_c = (0.5 m_d {U_d}^2 - 0.5 m_{cd} {U_{cd}}^2)/E_i, \quad (4)$$

where h_c, h_0, h_{rup} are the heights of the particle center at the moment of the droplet–particle contact, U_d, U_{cd} are the initial droplet velocity and child droplet velocity. F_p, F_{vis}, F_{sf} are the projections of the pressure, viscous drag and surface tension forces in the normal direction. E_p, E_{vis}, E_{sf} are the proportions of the kinetic dissipation energy caused by external forces. E_i is the initial kinetic energy.

For the transition from agglomeration to stretching separation to occur, the kinetic dissipation energy must be greater than or equal to 1. At $E_c > 1$, stretching separation is bound to occur, which is one of the prerequisites of using liquid in industrial applications.

A decrease in the surface tension and an increase in the viscosity of liquid lead to lower kinetic energy (E_i) and, thus, higher kinetic dissipation energy (E_c). This brings about stretching separation. The Equations (1)–(4) can be used to find the critical ratios of energies in the droplet–particle collision zone, at which the transition between the regimes occurs in the experiments with droplets colliding with particles and with each other. Since most technologies involve multicomponent and multiphase flows, it is important to differentiate between the regimes and critical conditions for the collisions of droplets with each other and droplets with solid particles. This research presents the experimental results for developing the existing models to take this differentiation into account.

4. Conclusions

(i) The results of the conducted experiments were generalized as collision regime maps for droplets and solid particles in the systems of B(We) and We(Oh) coordinates. Agglomeration and stretching separation regimes were distinguished. It was established how the liquid properties shift the transition boundaries between the collision regimes on the B(We) and We(Oh) maps. Approximations for a mathematical description of the transition boundaries between the agglomeration and stretching separation regimes were obtained. They took the form: $B = a \cdot We^2 + b \cdot We + c$, $We = a \cdot Oh + c$.

(ii) It was established that an increase in the liquid viscosity from 1.4 to 6.3 mPa·s increases the critical Weber number by 20–30% between the agglomeration and stretching separation regimes, and decreases the ratio of the free surface areas after and before the droplet-particle collision almost by 40%. A decrease in the surface tension from 72.69 to 36.1 mN/m shifts the boundary between agglomeration and stretching separation towards 25% lower We, as well as increases the ratios of the free surface areas after and before the droplet-particle collision by 45%. A decrease in the interfacial tension from 42.57 to 3.41 mN/m increases the ratios of the free surface areas after and before the collision of a droplet with a solid particle by almost 40% and decreases the critical Weber numbers for stretching separation by 20–30%.

(iii) The results are of interest for the development of secondary atomization technologies. They can be used to predict the conditions that are sufficient for the transition between the agglomeration and stretching separation regimes for liquids with varying dynamic viscosities, densities, surface and interfacial tensions.

Supplementary Materials: The following supporting information can be downloaded at: https://www.mdpi.com/article/10.3390/app122110747/s1, Video S1: Video-grams of a droplet-particle collision in the stretching separation regime when varying the liquid viscosity, Video S2: Video-grams of a droplet-particle collision in the stretching separation regime when varying the liquid surface tension; Video S3: Images of a droplet-particle collision in the stretching separation regime when varying the interfacial tension of liquid.

Author Contributions: Conceptualization, G.K. and N.S.; methodology, N.S. and A.I.; investigation, P.T., N.S. and A.I.; writing—original draft preparation, A.I., N.S., P.T. and G.K.; writing—review and editing, A.I., N.S., P.T. and G.K.; funding acquisition, P.T., N.S. and A.I. All authors have read and agreed to the published version of the manuscript.

Funding: The Research was supported by the Russian Science Foundation (project 18-71-10002-π, https://rscf.ru/en/project/21-71-03001/, accessed on 30 July 2021).

Conflicts of Interest: The authors declare no conflict of interest.

Nomenclature

B	dimensionless linear impact parameter:
b	distance between the centers of droplet-particle mass, mm;
Ca	capillary number;

E_c	kinetic dissipation energy, J;
E_i	initial kinetic energy, J;
E_p, E_{vis}, E_{sf}	proportions of the kinetic dissipation energy used by external forces;
F_p, F_{vis}, F_{sf}	projections of the pressure, viscous drag and surface tension forces in the normal direction, J;
h_c, h, h_{rup}	heights of the particle center at the moment of a droplet-particle contact, m.
m_{cd}	child droplet mass, kg;
m_d	droplet mass, kg;
N	number of droplets emerging as a result of interaction of two initial droplets, items;
Oh	Ohnesorge number;
p_{iz}	pressure difference at the interface;
R_d	droplet radius, mm;
r_{dn}	radius of the n-th child droplet, mm;
Re	Reynolds number;
R_p	particle radius, mm;
S_0	total surface area of a droplet before collision, m^2;
S_1	total surface area of liquid fragments resulting from droplet-particle interaction, m^2;
U_{cd}	child droplet velocity, m/s;
U_d	droplet velocity, m/s;
We	Weber number.
Greek symbols	
α	angle between droplet and particle, ^{o};
θ	contact angle, ^{o};
μ	dynamic viscosity, Pa·s;
ρ	density, kg/m^3;
σ	surface tension, N/m;
σ_0	interfacial tension, N/m.
Abbreviation	
A	agglomeration;
SS	stretching separation.

References

1. Rajesh, S.R.; Naveen, P.T.; Krishnakumar, K.; Ranjith, K.S. Dynamics of Single Droplet Impact on Cylindrically-Curved Superheated Surfaces. *Exp. Therm. Fluid Sci.* **2019**, *101*, 251–262. [CrossRef]
2. Jiao, Y.; Xue, X.; Ding, S.; Zhou, Q.; Tian, Y.; Liu, X.; Wang, S. Influence of Poly (Ethylene Glycol) 20,000 Concentration on Atomization and Deposition Characteristics of Nozzle. *Appl. Sci.* **2021**, *11*, 10513. [CrossRef]
3. Fujimoto, H.; Obana, W.; Ashida, M.; Hama, T.; Takuda, H. Hydrodynamics and Heat Transfer Characteristics of Oil-in-Water Emulsion Droplets Impinging on Hot Stainless Steel Foil. *Exp. Therm. Fluid Sci.* **2017**, *85*, 201–212. [CrossRef]
4. Azmi, W.H.; Sharma, K.V.; Mamat, R.; Najafi, G.; Mohamad, M.S. The Enhancement of Effective Thermal Conductivity and Effective Dynamic Viscosity of Nanofluids—A Review. *Renew. Sustain. Energy Rev.* **2016**, *53*, 1046–1058. [CrossRef]
5. Kahani, M.; Jackson, R.G.; Rosengarten, G. Experimental Investigation of TiO2/Water Nanofluid Droplet Impingement on Nanostructured Surfaces. *Ind. Eng. Chem. Res.* **2016**, *55*, 2230–2241. [CrossRef]
6. Zhou, J.; Wang, Y.; Geng, J.; Jing, D. Characteristic Oscillation Phenomenon after Head-on Collision of Two Nanofluid Droplets. *Phys. Fluids* **2018**, *30*, 072107. [CrossRef]
7. Sen, S.; Vaikuntanathan, V.; Sivakumar, D. Impact Dynamics of Alternative Jet Fuel Drops on Heated Stainless Steel Surface. *Int. J. Therm. Sci.* **2017**, *121*, 99–110. [CrossRef]
8. Shao, L.; Liu, D.; Ma, J.; Chen, X. Normal Collision between Partially Wetted Particles by Using Direct Numerical Simulation. *Chem. Eng. Sci.* **2022**, *247*, 117090. [CrossRef]
9. Tomar, V.; Bose, M. Anomalies in Normal and Oblique Collision Properties of Spherical Particles. *Powder Technol.* **2018**, *325*, 669–677. [CrossRef]
10. Yang, C.; Jeong, J.; Kim, Y.; Bang, B.; Lee, U. Numerical Simualtion of a Circulating Fluidized Bed Combustor and Evaluation of Empirical Models for Estimating Solids Volume Fraction. *Powder Technol.* **2021**, *393*, 786–795. [CrossRef]

11. Stefanitsis, D.; Malgarinos, I.; Strotos, G.; Nikolopoulos, N.; Kakaras, E.; Gavaises, M. Numerical Investigation of the Aerodynamic Breakup of Diesel and Heavy Fuel Oil Droplets. *Int. J. Heat Fluid Flow* **2017**, *68*, 203–215. [CrossRef]
12. Wang, Z.; Sun, T.; Yang, Z.; Zhu, G.; Shi, H. Interactions between Two Deformable Droplets in Tandem Fixed in a Gas Flow Field of a Gas Well. *Appl. Sci.* **2021**, *11*, 11220. [CrossRef]
13. Kovačević, A.G.; Petrović, S.; Mimidis, A.; Stratakis, E.; Pantelić, D.; Kolaric, B. Molding Wetting by Laser-Induced Nanostructures. *Appl. Sci.* **2020**, *10*, 6008. [CrossRef]
14. Zhuravlev, E.; Jiang, J.; Zhou, D.; Androsch, R.; Schick, C. Extending Cooling Rate Performance of Fast Scanning Chip Calorimetry by Liquid Droplet Cooling. *Appl. Sci.* **2021**, *11*, 3813. [CrossRef]
15. Heidari, E.; Sobati, M.A.; Movahedirad, S. Dynamics of Particle Wetting in Wet Granulation: Micro-Scale Analysis. *Int. J. Heat Mass Transf.* **2020**, *146*, 118853. [CrossRef]
16. Tabeei, A.; Samimi, A.; Mohebbi-Kalhori, D. CFD Modeling of an Industrial Scale Two-Fluid Nozzle Fluidized Bed Granulator. *Chem. Eng. Res. Des.* **2020**, *159*, 605–614. [CrossRef]
17. Fathinia, F.; Khiadani, M.; Al-Abdeli, Y.M. Experimental and Mathematical Investigations of Spray Angle and Droplet Sizes of a Flash Evaporation Desalination System. *Powder Technol.* **2019**, *355*, 542–551. [CrossRef]
18. Anufriev, I.S.; Baklanov, A.M.; Borovkova, O.V.; Vigriyanov, M.S.; Leshchevich, V.V.; Sharypov, O.V. Investigation of Soot Nanoparticles during Combustion of Liquid Hydrocarbons with Injection of a Superheated Steam Jet into the Reaction Zone. *Combust. Explos. Shock Waves* **2017**, *53*, 140–148. [CrossRef]
19. Fröhlich, J.A.; Raiber, T.V.; Hinrichs, J.; Kohlus, R. Nozzle Zone Agglomeration in Spray Dryers: Influence of Total Solid Content on Agglomerate Properties. *Powder Technol.* **2021**, *390*, 292–302. [CrossRef]
20. Yu, H.; Jin, Y.-C.; Cheng, W.; Yang, X.; Peng, X.; Xie, Y. Multiscale Simulation of Atomization Process and Droplet Particles Diffusion of Pressure-Swirl Nozzle. *Powder Technol.* **2021**, *379*, 127–143. [CrossRef]
21. Breitenbach, J.; Roisman, I.V.; Tropea, C. From Drop Impact Physics to Spray Cooling Models: A Critical Review. *Exp. Fluids* **2018**, *59*, 55. [CrossRef]
22. Wijshoff, H. Drop Dynamics in the Inkjet Printing Process. *Curr. Opin. Colloid Interface Sci.* **2018**, *36*, 20–27. [CrossRef]
23. Pawar, S.K.; Henrikson, F.; Finotello, G.; Padding, J.T.; Deen, N.G.; Jongsma, A.; Innings, F.; Kuipers, J.A.M.H.; Hans Kuipers, J.A.M. An Experimental Study of Droplet-Particle Collisions. *Powder Technol.* **2016**, *300*, 157–163. [CrossRef]
24. Mitra, S.; Evans, G.M.; Doroodchi, E.; Pareek, V.; Joshi, J.B. Interactions in Droplet and Particle System of near Unity Size Ratio. *Chem. Eng. Sci.* **2017**, *170*, 154–175. [CrossRef]
25. Malgarinos, I.; Nikolopoulos, N.; Gavaises, M. A Numerical Study on Droplet-Particle Collision Dynamics. *Int. J. Heat Fluid Flow* **2016**, *61*, 499–509. [CrossRef]
26. Mitra, S.; Sathe, M.J.; Doroodchi, E.; Utikar, R.; Shah, M.K.; Pareek, V.; Joshi, J.B.; Evans, G.M. Droplet Impact Dynamics on a Spherical Particle. *Chem. Eng. Sci.* **2013**, *100*, 105–119. [CrossRef]
27. Pasternak, L.; Mañas, M.J.M.; Sommerfeld, M. Influence of Droplet Properties on the Coating of Free-Falling Spherical Particles. *At. Sprays* **2021**, *31*, 37–61. [CrossRef]
28. Sechenyh, V.; Amirfazli, A. An Experimental Study for Impact of a Drop onto a Particle in Mid-Air: The Influence of Particle Wettability. *J. Fluids Struct.* **2016**, *66*, 282–292. [CrossRef]
29. Hu, M.; Zhou, J.; Li, Y.; Zhuo, X.; Jing, D. Effects of the Surface Wettability of Nanoparticles on the Impact Dynamics of Droplets. *Chem. Eng. Sci.* **2021**, *246*, 116977. [CrossRef]
30. Zhao, P.; Hargrave, G.K.; Versteeg, H.K.; Garner, C.P.; Reid, B.A.; Long, E.J.; Zhao, H. The Dynamics of Droplet Impact on a Heated Porous Surface. *Chem. Eng. Sci.* **2018**, *190*, 232–247. [CrossRef]
31. Yoon, I.; Shin, S. Direct Numerical Simulation of Droplet Collision with Stationary Spherical Particle: A Comprehensive Map of Outcomes. *Int. J. Multiph. Flow* **2021**, *135*, 103503. [CrossRef]
32. Zheng, Y.; Huang, Z.; Zhang, C.; Wu, Z. Hydrophobic Antiwetting of Aquatic UAVs: Static and Dynamic Experiment and Simulation. *Appl. Sci.* **2022**, *12*, 7626. [CrossRef]
33. Hirschler, M.; Oger, G.; Nieken, U.; Le Touzé, D. Modeling of Droplet Collisions Using Smoothed Particle Hydrodynamics. *Int. J. Multiph. Flow* **2017**, *95*, 175–187. [CrossRef]
34. Tang, C.; Qin, M.; Weng, X.; Zhang, X.; Zhang, P.; Li, J.; Huang, Z. Dynamics of Droplet Impact on Solid Surface with Different Roughness. *Int. J. Multiph. Flow* **2017**, *96*, 56–69. [CrossRef]
35. Yoon, I.; Shin, S. Computational Study on Dynamic Behavior during Droplet-Particle Interaction. *Chem. Eng. Sci.* **2021**, *241*, 116656. [CrossRef]
36. Vilela, V.; de Souza, F.J. A Numerical Study on Droplet-Particle Collision: Lamella Characterization. *Flow Turbul. Combust.* **2020**, *105*, 965–987. [CrossRef]
37. Milacic, E.; Baltussen, M.W.; Kuipers, J.A.M. Direct Numerical Simulation Study of Droplet Spreading on Spherical Particles. *Powder Technol.* **2019**, *354*, 11–18. [CrossRef]
38. Tkachenko, P.P.; Shlegel, N.E.; Volkov, R.S.; Strizhak, P.A. Experimental Study of Miscibility of Liquids in Binary Droplet Collisions. *Chem. Eng. Res. Des.* **2021**, *168*, 1–12. [CrossRef]
39. Tkachenko, P.P.; Shlegel, N.E.; Strizhak, P.A. Collisions of Water Droplets in the High-Temperature Air. *Int. J. Heat Mass Transf.* **2021**, *170*, 121011. [CrossRef]

40. Kropotova, S.; Strizhak, P. Collisions of Liquid Droplets in a Gaseous Medium under Conditions of Intense Phase Transformations: Review. *Energies* **2021**, *14*, 6150. [CrossRef]
41. Qin, C.; He, Y.; Shi, B.; Zhao, T.; Lv, F.; Cheng, X. Experimental Study on Breakdown Characteristics of Transformer Oil Influenced by Bubbles. *Energies* **2018**, *11*, 634. [CrossRef]
42. Šikalo, Š.; Marengo, M.; Tropea, C.; Ganić, E.N. Analysis of Impact of Droplets on Horizontal Surfaces. *Exp. Therm. Fluid Sci.* **2002**, *25*, 503–510. [CrossRef]
43. Negeed, E.-S.R.; Ishihara, N.; Tagashira, K.; Hidaka, S.; Kohno, M.; Takata, Y. Experimental Study on the Effect of Surface Conditions on Evaporation of Sprayed Liquid Droplet. *Int. J. Therm. Sci.* **2010**, *49*, 2250–2271. [CrossRef]
44. Fujimoto, H.; Tong, A.Y.; Takuda, H. Interaction Phenomena of Two Water Droplets Successively Impacting onto a Solid Surface. *Int. J. Therm. Sci.* **2008**, *47*, 229–236. [CrossRef]
45. Shlegel, N.E.; Tkachenko, P.P.; Strizhak, P.A. Influence of Viscosity, Surface and Interfacial Tensions on the Liquid Droplet Collisions. *Chem. Eng. Sci.* **2020**, *220*, 115639. [CrossRef]
46. Williams, Y.O.; Roas-Escalona, N.; Rodríguez-Lopez, G.; Villa-Torrealba, A.; Toro-Mendoza, J. Modeling Droplet Coalescence Kinetics in Microfluidic Devices Using Population Balances. *Chem. Eng. Sci.* **2019**, *201*, 475–483. [CrossRef]
47. *Standard Test Method for Kinematic Viscosity of Transparent and Opaque Liquids (And Calculation of Dynamic Viscosity)*; ASTM International: West Conshohocken, PA, USA, 2006.
48. Lunkenheimer, K.; Wantke, K.D. On the Applicability of the Du Nouy (Ring) Tensiometer Method for the Determination of Surface Tensions of Surfactant Solutions. *J. Colloid Interface Sci.* **1978**, *66*, 579–581. [CrossRef]
49. Koh, Y.T.; Higgins, A.S.; Weber, S.J.; Kast, W. Immunological Consequences of Using Three Different Clinical/Laboratory Techniques of Emulsifying Peptide-Based Vaccines in Incomplete Freund's Adjuvant. *J. Transl. Med.* **2006**, *4*, 42. [CrossRef]
50. Wood, J.H.; Catacalos, G.; Lieberman, S. V Adaptation of Commercial Viscometers for Special Applications in Pharmaceutical Rheology I: The Brookfield Viscometer. *J. Pharm. Sci.* **1963**, *52*, 296–298. [CrossRef]
51. Tkachenko, P.P.; Shlegel, N.E.; Strizhak, P.A. Interaction between droplets of solutions in a heated gaseous medium. *Powder Technol.* **2021**, *390*, 86–96. [CrossRef]
52. Qian, J.; Law, C.K. Regimes of Coalescence and Separation in Droplet Collision. *J. Fluid Mech.* **1997**, *331*, 59–80. [CrossRef]
53. Liu, R.; Zhou, G.; Wang, K.; Niu, C.; Zhang, Q.; Wang, Y.; Dong, X.; Ramakrishna, S. Experimental Investigation on Highly Efficient Collection and Cleaning for Fine Coal Dust Particles by Dry-Wet Mixed Chemical Method. *J. Environ. Chem. Eng.* **2021**, *9*, 105861. [CrossRef]
54. Arya, S.; Novak, T. Numerical Investigation of the Effect of a Novel Wet Scrubber on Dust Reduction in an Underground Coal Mine. *Mining Metall. Explor.* **2020**, *37*, 129–139. [CrossRef]
55. Khatri, D.; Yang, Z.; Li, T.; Axelbaum, R.L. Development of an Aerosol Sampler for Pressurized Systems and Its Application to Investigate the Effect of Residence Time on PM1 Formation in a 15 Bar Oxy-Coal Combustor. *Aerosol Sci. Technol.* **2021**, *55*, 438–448. [CrossRef]
56. Volkov, R.S.; Kuznetsov, G.V.; Strizhak, P.A. Water Droplet Deformation in Gas Stream: Impact of Temperature Difference between Liquid and Gas. *Int. J. Heat Mass Transf.* **2015**, *85*, 1–11. [CrossRef]
57. Demidovich, A.V.; Kropotova, S.S.; Piskunov, M.V.; Shlegel, N.E.; Vysokomornaya, O.V. The Impact of Single- and Multicomponent Liquid Drops on a Heated Wall: Child Droplets. *Appl. Sci.* **2020**, *10*, 942. [CrossRef]